40 CFR Part 191
Subparts B and C
Compliance Recertification Application 2026
for the
Waste Isolation Pilot Plant

Appendix PORSURF-2026
Porosity Surface

United States Department of Energy
Waste Isolation Pilot Plant

Carlsbad Field Office
Carlsbad, New Mexico

Compliance Recertification Application 2026
Appendix PORSURF-2026

TABLE OF CONTENTS

PORSURF-1.0 INTRODUCTION 1

PORSURF-2.0 CREEP CLOSURE CONCEPTUAL MODEL FOR WASTE-FILLED AREAS 5

PORSURF-3.0 CREEP CLOSURE MODEL FOR WASTE-FILLED AREAS 6

PORSURF-4.0 INTERPOLATION OF THE CREEP CLOSURE MODEL PREDICTIONS FOR WASTE-FILLED AREAS 10

PORSURF-5.0 TREATMENT OF NON-WASTE-FILLED AREAS 13

PORSURF-6.0 REFERENCES 14

LIST OF FIGURES

Figure PORSURF- 1. Gas Generation (Top Plot), Fluid Pressure (Middle Plot), and Porosity Histories (Bottom Plot) for Various Values of the Scaling Factor *f* 9
Figure PORSURF- 2. Interpolation Method to Determine Porosity as a Function of Time and Pressure 10
Figure PORSURF- 3. Triangular Interpolation to Determine the Porosity at (*t*, *p*) 11

ACRONYMS AND ABBREVIATIONS

A	area of triangle used in porosity surface interpolation
CCA	Compliance Certification Application
CFR	Code of Federal Regulations
CRA	Compliance Recertification Application
DOE	U.S. Department of Energy
DRZ	disturbed rock zone
EPA	U.S. Environmental Protection Agency
ROM	run-of-mine
f	scaling factor for the gas generation rate
$f_{\max}$	maximum scaling factor for the gas generation rate
k	permeability
n_g	number of moles of gas
n_g^{pot}	potential number of moles of gas
Mmol	megamole
MPa	megapascals
p	fluid pressure
p_{ls}	lithostatic pressure at the repository horizon
PA	Performance Assessment
POP	Pipe Overpack
ϕ	Lagrangian porosity, averaged over the original room volume
t	time
V_v	void volume
V_{r0}	original room volume
WIPP	Waste Isolation Pilot Plant
yr	year

PORSURF-1.0 INTRODUCTION

This appendix to the 2026 Compliance Recertification Application (CRA-2026) describes how creep closure is incorporated into the CRA-2026 Performance Assessment (PA) of the Waste Isolation Pilot Plant (WIPP) nuclear waste repository. This first section presents the phenomenon of creep closure, the concept of a porosity (response) surface, and past studies related to the porosity surface. After these preliminaries, this section presents a list of the remaining topics covered by the appendix.

The ability of salt to deform over time, eliminate void space within a room, and create an impermeable barrier around the waste is one of the primary reasons the U.S. Department of Energy (DOE) located the WIPP repository in the Salado salt formation (NAS-NRC 1957, pp. 4, 5). Each room at the WIPP will naturally close in around its contents, which may include waste containers, brine, and gases. The contents supply back pressure that slows the rate of closure. The room will gradually stop evolving as the back pressure supplied by the room contents asymptotically approaches lithostatic pressure. Creep closure affects the effective porosity (interconnected pore space/bulk volume) available to transport fluids (brine and gases). It also affects the absolute porosity (total pore space/bulk volume) available to store fluids. These fluids can carry radionuclides within and away from the repository in certain PA scenarios.

Ideally, the WIPP PA would perform fully coupled simulations of creep closure, gas generation, and fluid transport to predict the potential flow of radionuclides. The PA, however, must perform thousands of gas generation and two-phase (brine and gas) flow simulations, called Salado fluid flow simulations. Thousands of fully coupled creep closure and Salado fluid flow simulations are not tractable with the current combination of software and hardware qualified for use by the PA. Instead, the PA uses an uncoupled approach to link the creep closure simulations to the Salado fluid flow simulations.

In the uncoupled approach, a series of creep closure simulations is performed, followed by a series of Salado fluid flow simulations. The creep closure simulations include the mechanical behavior of the rock mass, the waste, and the gas. (The brine is ignored in the creep closure simulations for simplicity.) The gas generation history, however, is prescribed a priori, and the gas is not permitted to escape from the room. Each creep closure simulation utilizes a different multiple of the maximum expected gas generation history to compute a set of porosity and gas pressure histories. These histories are used to construct a porosity (response) surface, in which porosity is expressed as a function of time and gas pressure in the room. The Salado fluid flow simulations use the porosity surface as a “interpolation table” to determine the volume available to store fluids (gases and brine) at a given fluid pressure and time.

The porosity surface must be able to respond to any valid fluid pressure—time pair given to it because the fluid pressure is controlled by the Salado fluid flow model, not the porosity surface. For example, if the fluid pressure is high enough in some part of the repository, then the Salado fluid flow model controls whether fluid can escape through fractured anhydrite marker beds or other pathways. If outflow through those pathways is too slow relative to inflow and gas

generation, then the fluid pressure may exceed lithostatic pressure and the porosity surface should predict that the room will expand. Room expansion is uncommon, but it does occur in some PA scenarios.

The current combination of qualified software and hardware is well-suited for modeling gradual creep closure, but it cannot credibly model a roof fall or the subsequent creep closure. Roof falls are likely to occur in non-waste-filled areas due to the lack of room contents to support the roof. Non-waste-filled areas are defined as the north end of the repository (i.e. the experimental regions), operational region, west operational region, and abandoned panel closures (see Appendix PA, Figure PA-1 and PA-12). Rock bolts can delay roof falls in non-waste-filled areas for many years, but these bolts will ultimately fail, and the roof should eventually fall if they are not replaced. This sequence occurred in 2016 after access to the WIPP underground was severely restricted for several years: salt blocks detached from the roof and fell several meters onto the floor, creating rubble piles on the floor (see Reedlunn et al., 2019, Figure 1-3). If fluid pressures remain sufficiently low, creep closure should eventually cause these rubble piles to reconsolidate into nearly solid salt, but it is difficult to estimate how long reconsolidation will take. For example, reconsolidation models would need to be calibrated or validated against experiments, yet it is impractical to measure the reconsolidation of rubble with meter-sized boulders in the laboratory. As a result, the PA treats non-waste-filled areas differently than waste-filled areas, as discussed in Appendix PORSURF-5.0, and uses a gradual creep closure model focused on waste-filled rooms. Waste-filled rooms are less likely to have roof falls and, if they do occur, their impact is expected to be small (see Appendix PORSURF-2.0).

Stone (1997) constructed the original creep closure model and computed the first porosity surface. He considered rooms filled with standard 55-gallon waste containers and pressurized fluids, and he ignored the possibility of roof falls. The Stone (1997) surface was used in the Compliance Certification Application (CCA) (U.S. DOE 1996) and in each CRA, through CRA-2019 (U.S. DOE 2019). Despite the repeated use of this porosity surface, other porosity surfaces have been considered over the years.

In 2004, Park and Holland (2007)[1] studied the impact of mining disposal rooms 2.43 m higher, such that the ceilings of these upper horizon rooms were coincident with Clay Seam G. They found this change had a relatively minor impact on room porosity, so the compliance applications continued to use the Stone (1997) porosity surface for simplicity.

In 2005, Park and Hansen (2005) computed porosity surfaces for rooms filled with different types of waste containers. They considered a room filled with 6-inch Pipe Overpack (POP) containers, a room filled with 12-inch POP containers, a room filled with super-compacted waste, a room filled with 1/3 super-compacted waste and 2/3 standard waste, and a room filled with 2/3 super-compacted waste and 1/3 standard waste. The super-compacted and POP waste forms tended to hold open the rooms, resulting in significantly greater room porosity than

[1] Park and Holland originally released their study as SAND2003-3409 in January 2004, but they later released a corrected version as SAND2007-3334 in September 2007.

rooms full of standard waste containers. As an aside, the Park and Hansen (2005) model for the POP containers was later found to be far too stiff (see Reedlunn and Bean, 2019, pg. 27, and Reedlunn and Bean, 2024, Section 4.2.3), so the POP porosity response surfaces in Park and Hansen (2005) should be considered an upper bound.

Hansen et al. (2004) studied how a heterogenous distribution of the waste forms considered in Park and Hansen (2005) might impact WIPP's performance. Their analysis statistically sampled from four different porosity surfaces, each corresponding to one of four waste container types: standard 55-gallon containers, 6-inch POP containers, 12-inch POP containers, and super-compacted containers. These four waste container types represented various bounding combinations of waste package rigidity and waste initial porosity. The analysis found that increasing waste strength did not significantly increase radionuclide releases. This conclusion was used to justify the repeated usage of the Stone (1997) porosity surface in subsequent compliance applications.

More recent studies, however, identified several deficiencies in the Stone (1997) creep closure model. For example, Reedlunn et al. (2022, Section 3.5) showed that the model under-predicted room closure rates 5.7 years after room excavation by a factor of 2.48. Jensen et al. (2023, Section 1.4) also demonstrated that the model predicted tensile out-of-plane stresses in the waste that should have been compressive. See Vignes et al. (2023, Chapter 2) for a more comprehensive summary of the Stone (1997) model deficiencies.

As a result, Vignes et al. (2023) made several changes to the creep closure model to resolve the Stone (1997) model deficiencies. (A brief summary of the changes is provided in Appendix PORSURF-3.0.) Like Stone (1997), Vignes et al. (2023) considered rooms filled with standard 55-gallon waste containers and fluids, and they did not consider roof falls. The Vignes et al. (2023) changes, nevertheless, substantially improved the model's scientific basis, and improved the model's ability to capture laboratory and field experiments. The resulting porosity surface is less sensitive to fluid pressure and returns lower porosities than the Stone (1997) porosity surface when the fluid pressure remains beneath lithostatic pressure.

Day (2025) used the PA model corresponding to the Replacement Panels Planned Change Request to compare radionuclide releases associated with the Stone (1997) and Vignes et al. (2023) porosity surfaces. He found that the Vignes et al. (2023) porosity surface increased mean total releases by factors of 1.6 and 2.4 at the 0.1 and 0.001 compliance limit probabilities, respectively.

This newfound sensitivity to porosity appears to contradict the finding of Hansen et al. (2004), but the sensitivity is likely explained by the following two factors. First, the alternative porosity surfaces considered by Hansen et al. (2004) predicted equal or higher porosities than those from the Stone (1997) surface, while the Vignes et al. (2023) porosity surface predicts porosities lower than the those from the Stone (1997) surface. Releases could be insensitive to raising the porosity, but sensitive to lowering the porosity. Second, numerous other changes besides the Vignes et al. (2023) porosity surface were made to the WIPP PA model between 2004 and 2025.

The newfound sensitivity could be due to the interaction of the Vignes et al. (2023) porosity surface with those other changes.

If the Hansen et al. (2004) analysis were rerun with today's PA model, the expectation is the higher porosities associated with stronger waste containers would lead to equivalent or decreased releases. Consequently, the PA only uses the Vignes et al. (2023) porosity surface for waste-filled areas to conservatively overestimate releases.

The final topic discussed in this section is the accuracy of the uncoupled approach. Rock salt viscoplasticity is path-dependent, meaning its response depends on its current deformation *and* the past sequence of deformations it experienced. The uncoupled approach, on the other hand, largely ignores this path-dependence. Freeze et al. (1995) and Freeze (1996) found that the uncoupled approach was sufficiently accurate, when the Salado fluid flow simulations used fluid pressurization histories similar to those used to construct the porosity surface, or pressures remained low enough that room expansion did not occur. The Salado fluid flow simulations, however, are not constrained to follow the same pressure histories used to construct the porosity surface or remain low, so Reedlunn et al. (2025) assessed the errors associated with the uncoupled approach. They considered 600 different pressure histories derived from a series of Salado fluid flow simulations. These 600 representative pressure histories were input into the Vignes et al. (2023) creep closure model and porosity surface to compute 600 porosity error histories. When the porosity error was averaged within 0.2 MPa width pressure bins, this average error was 1.3 % when the fluid pressure remained below lithostatic pressure but became as large as 79.3 % when the pressure exceeded lithostatic. In response to the errors at high pressures, a preliminary study of the PA's sensitivity to these porosity errors was conducted. The study modified the Vignes et al. (2023) porosity surface by artificially limiting the porosity to less than 0.09 when the pressure was above lithostatic. When the PA used this artificially limited porosity surface the largest porosity error, averaged over a 0.2 MPa bin, decreased by a factor of 0.35 yet radionuclide releases changed by an imperceptible amount. This result suggests that the porosity errors at high pressures have a negligible impact on releases.

The remainder of this appendix reviews the creep closure conceptual model for waste-filled areas, the creep closure model for waste-filled areas, how the porosity surface is interpolated in the Salado fluid flow simulations, and how the Salado fluid flow simulations treat non-waste-filled areas of the repository.

PORSURF-2.0 CREEP CLOSURE CONCEPTUAL MODEL FOR WASTE-FILLED AREAS

The description of the creep closure conceptual model in this section is equivalent to the original creep closure conceptual model used in the CCA (U. S. DOE 1996, Section 6.4.3.1 and Appendix PEER 1, Section 3.19.1)[2]. This conceptual model was found reasonable and adequate by the Conceptual Models Peer Review in 1996 (U. S. DOE 1996, Appendix PEER 1, Section 3.19.2), and it has been used in all subsequent compliance applications, including CRA-2019 (U.S. DOE 2019). The conceptual model is described again below to re-introduce the assumptions regarding room expansion and roof falls, which were mistakenly omitted from past versions of Appendix PORSURF. Less importantly, the description below improves on the CCA description in several ways: it omits extraneous information about geochemistry, geohydraulics, and implementation details; it clearly calls out the model assumptions; and it clarifies a few technical points.

The creep closure conceptual model assumes that room closure occurs because lithostatic pressure at the room horizon exceeds the back pressure from the room contents. This pressure difference leads to deviatoric (shear) stresses in the surrounding rock, causing it to deform. The rate of room closure depends on the lithostatic pressure, the geomechanical behavior of the surrounding rock, and the mechanical behavior of the room contents. The room contents are assumed to be waste containers and/or fluids, such as brine and/or gases. The closure process gradually comes to a halt once the back pressure asymptotically approaches lithostatic pressure, making the deviatoric stress in the salt negligible.

If geochemical or geohydraulic processes happen to cause the back pressure to exceed lithostatic pressure, the conceptual model assumes the room expands until the back pressure approaches lithostatic pressure. The rate of expansion is controlled by the same factors that govern room closure.

The conceptual model assumes waste-filled rooms close gradually and do not have roof falls. This assumption is questionable for non-waste-filled rooms, where roof falls are likely, so the conceptual model is not designed for such areas. The assumption is, nevertheless, expected to be valid for waste-filled rooms, where the waste can support the roof and prevent most roof falls. If a block of salt still detaches from the roof, the block will not fall far before landing on the waste. One can, therefore, expect that partially and fully detached blocks would mate up fairly-well with the surrounding rock formation as the room closes. For these reasons, the error caused by ignoring roof falls in waste-filled rooms is assumed to be acceptably small.

The assumptions adopted by the creep closure conceptual model can be further illuminated by considering four possibilities for the room contents:

[2] The creep closure conceptual model description is spread out between two sections in the CCA (U. S. DOE 1996, Section 6.4.3.1 and Appendix PEER 1, Section 3.19.1), and it includes model implementation details that do not belong in a conceptual model. McCormick et al. (2024, Section 21) consolidates and reiterates the relevant portions of the conceptual model description without the unnecessary implementation details.

1. If a room contains no waste and fluids are allowed to easily escape the room, closure will proceed until the void volume created by the excavation is virtually eliminated.

2. If a room contains waste and fluids can easily escape, the room will close, contact the waste, and the rate of closure will decrease as the waste compacts and stiffens. Closure will eventually cease when the waste can counteract the pressure of the surrounding rock without further deformation.

3. If a room contains no waste and fluids cannot easily escape, the initially rapid rate of closure will gradually decrease as the fluid pressure asymptotically approaches lithostatic pressure. If the fluid pressure exceeds lithostatic pressure, the room will expand until the fluid pressure approaches lithostatic pressure.

4. If a room contains waste and fluids, they can resist the room closure together. In this process, the waste can be considered as a skeleton structure immersed in a pore fluid. If pore fluid pressures increase/decrease, less/more lithostatic pressure is carried by the skeleton, and more/less lithostatic pressure is carried by the fluid. If the pore pressure exceeds lithostatic pressure, the skeleton will fully unload, and the pore space will expand until the pore pressure asymptotically approaches lithostatic pressure.

PORSURF-3.0 CREEP CLOSURE MODEL FOR WASTE-FILLED AREAS

The PA uses the Vignes et al. (2023) creep closure model for waste-filled areas. This model is the current implementation of the creep closure conceptual model described in Appendix PORSURF-2.0. This section briefly introduces the Vignes et al. (2023) model, the improvements over the preceding Stone (1997) model, the software utilized in the simulations, and the simulation results. Further details of the model, improvements, sensitivity studies, and comparisons against the Stone (1997) results can be found in Vignes et al. (2023).

The creep closure model comprises three submodels: a geomechanical submodel, a waste compaction submodel, and a gas pressurization submodel. These three submodels combine to predict the void volume $V_v = V_v(t, f)$ available to store gas within the room at time t and with gas generation factor f.

The following details of the gas pressurization model are needed to understand how the creep closure predictions are incorporated into the Salado fluid flow simulations. As part of the uncoupled approach described in Appendix PORSURF-1.0, the gas pressurization model does not permit gas to escape the room. The amount of gas within the room $n_g = n_g(t, f)$ is prescribed a priori as

$$n_g = f\, n_g^{pot}, \qquad \text{Equation (PORSURF.1)}$$

where $0 \leq f \leq 1$ and $n_g^{pot} = n_g^{pot}(t)$ is the potential gas generation, which is designed to bound all gas generation realizations considered in the Salado fluid flow simulations. The $f = 1$ curve in the top plot of Figure PORSURF-1 depicts the n_g^{pot} function. Each creep closure simulation uses a different value of f to compute a pressure and porosity history. These histories are combined to create the porosity surface (see Appendix PORSURF-4.0). The gas pressure $p = p(t, f)$ is assumed to be spatially uniform throughout the room, including inside the waste pore space, so it is easily computed from V_v, n_g, and the temperature of the room using the ideal gas law.

The room porosity $\phi = \phi(t, f)$ is computed from void volume V_v and the original volume of the room V_{r0} as

$$\phi = \frac{V_v}{V_{r0}}. \qquad \text{Equation (PORSURF.2)}$$

In other words, ϕ is the pointwise Lagrangian porosity averaged over the original volume of the room. The terms Lagrangian porosity and Eulerian (intrinsic) porosity are commonly used in the poro-mechanics literature (e.g., Coussy 2010, Chapter 3) to refer to the ratio of void volume to the initial volume and the ratio of void volume to the current volume, respectively. The Salado fluid flow simulations only use the average Lagrangian porosity ϕ so Eulerian porosity will not be discussed further herein.

The Vignes et al. (2023) creep closure model contains the following improvements over the Stone (1997) model. The improved geomechanical submodel uses a more detailed stratigraphy, an enhanced salt constitutive model that captures salt's low-stress creep behavior, and a frictional sliding model for clay seams. The improved waste compaction submodel is based on new experiments that included both axial and lateral strain measurements on containers filled with a more representative waste composition. The improved gas pressurization submodel modifies n_g^{pot} by accounting for molecular hydrogen (H_2) generated from brine radiolysis and revising the other gas generation sources. In addition, the new creep closure model uses a more accurate numerical implementation that includes a finer mesh selected via a mesh convergence study.

The improvements implemented by Vignes et al. (2023) do not constitute departures from the creep closure conceptual model. All the same concepts and assumptions are involved. The improvements are based on new, more accurate, information than was available for the original Stone (1997) model.

The Vignes et al. (2023) simulations were performed using Sierra/SolidMechanics version 5.4.1 (Sierra/SolidMechanics 2022). The domain was discretized using finite elements, and the momentum balance equations were solved using explicit time integration with viscoplastic scaling.

The curves in Figure PORSURF-1 correspond to those presented in Vignes et al. (2023, Figures 2-5b, 3-7, and 3-5b). Each curve corresponds to an individual simulation with a certain value of f. The lithostatic pressure at the repository horizon $p_{ls} = 14.9$ MPa is labeled in the middle plot for reference. Note that the fluid pressure and porosity curves in Figure PORSURF-1 cannot be directly compared against the corresponding curves in Stone (1997, Figures 7 and 8) because n_g^{pot} is substantially different in each case. Instead, see Vignes et al. (2023, Section 3.3) for a proper comparison of the two porosity surfaces.

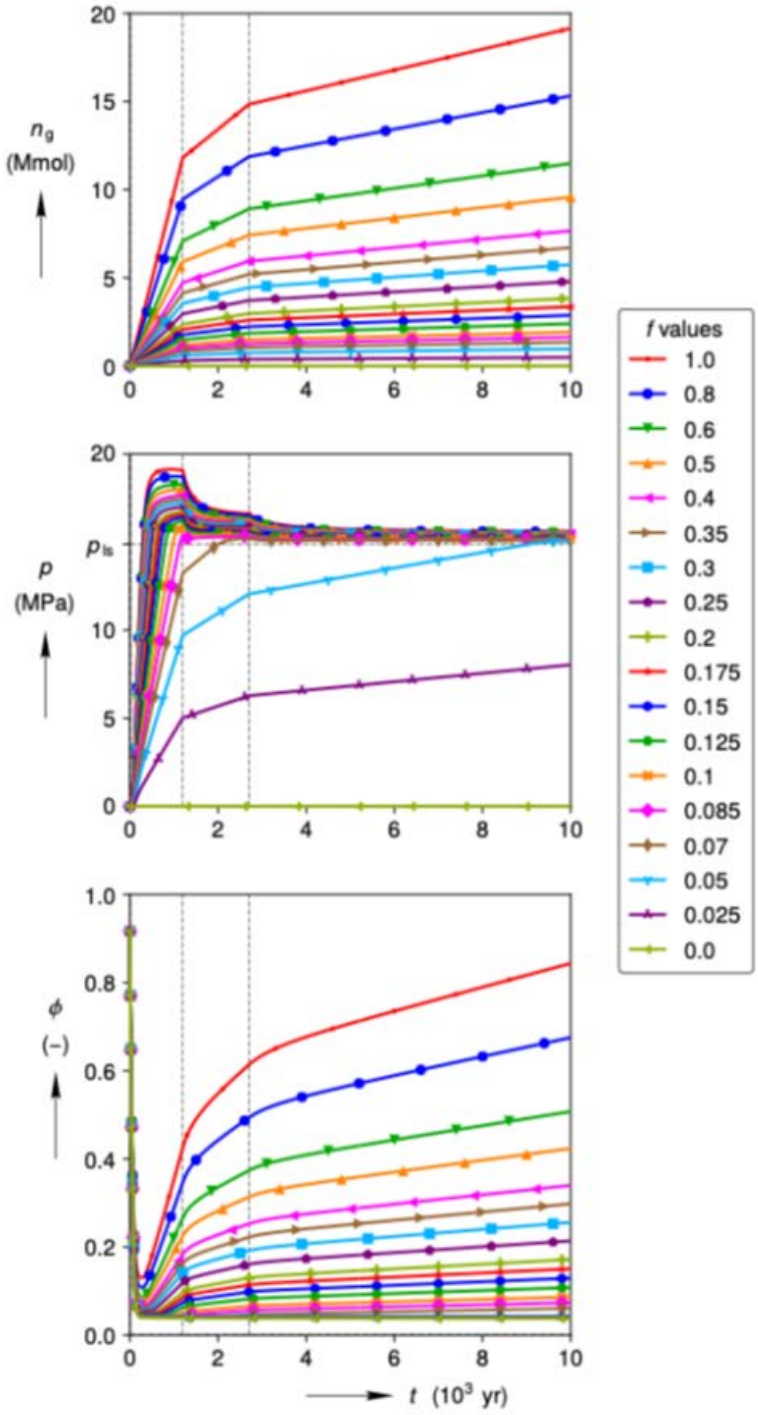


Figure PORSURF- 1**. Gas Generation (Top Plot), Fluid Pressure (Middle Plot), and Porosity Histories (Bottom Plot) for Various Values of the Scaling Factor *f*.**

PORSURF-4.0 INTERPOLATION OF THE CREEP CLOSURE MODEL PREDICTIONS FOR WASTE-FILLED AREAS

This section details how the Salado fluid flow simulations interpolate between the pressure and porosity curves in Figure PORSURF- 1 to obtain the waste-filled room porosity ϕ at arbitrary fluid pressure and time coordinate pairs. This interpolation effectively converts the curves into a porosity response surface. The interpolation procedure is the same as that used in CRA-2019 (U.S. DOE 2019, Appendix PORSURF-4.0). The description is revised below only to improve clarity.

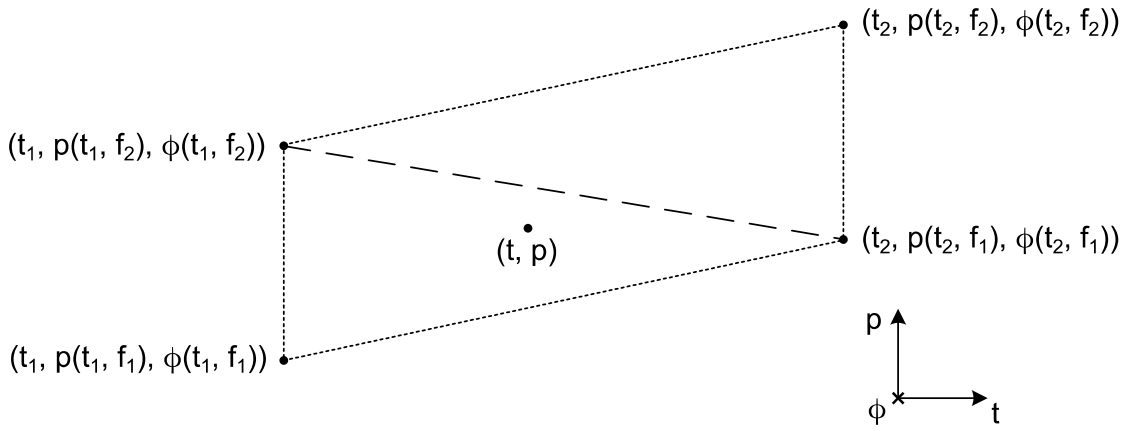


Figure PORSURF- 2. Interpolation Method to Determine Porosity as a Function of Time and Pressure.

The interpolation method consists of the following steps:

1. Although each pressure curve and each porosity curve in Figure PORSURF- 1 is depicted as continuous with respect to time, they actually consist of porosity and pressure values at discrete times. The Salado fluid flow model must, therefore, first find the two neighboring times t_1 and t_2 in the porosity predictions that bracket the given time t, i.e. $t_1 \leq t \leq t_2$.

2. Next, the Salado fluid flow model compares the current pressure *p* against the pressure data in the interpolation table corresponding to the maximum f value, $f_{\max}$. If *p* lies above the line formed by the points $(t_1, p(t_1, f_{\max}))$ and $(t_2, p(t_2, f_{\max}))$, the (Lagrangian) porosity ϕ is calculated as

$$\phi = \phi(t_1, f_{\max}) + \frac{\phi(t_2, f_{\max}) - \phi(t_1, f_{\max})}{t_2 - t_1}(t - t_1). \qquad \text{Equation (PORSURF.3)}$$

This approach interpolates the porosity with respect to time but avoids extrapolation with respect to pressure by using the temporally interpolated values as an upper limit.

In CRA-2026, p exceeded the $p(t_i, f_{\text{max}})$ data points by less than 0.13 MPa only during $0 \le t \le 30$ yr (see Day and King 2025, Section 5.3), which has a negligible impact on porosities. No lower pressure limit is required because $p \ge 0$ and $f = 0$ corresponds to $p = 0$.

3. For values of p less than the $p(t_i, f_{\text{max}})$ data points, the Salado fluid flow model finds f values f_1 and f_2 so that the point (t, p) lies between one line, defined by the points $\left(t_1, p(t_1, f_1)\right)$ and $\left(t_2, p(t_2, f_1)\right)$, and another line, defined by the points $\left(t_1, p(t_1, f_2)\right)$ and $\left(t_2, p(t_2, f_2)\right)$. This scenario is illustrated in Figure PORSURF- 2, which contains two triangles defined by neighboring points in the pressure—time plane.

4. Interpolation is performed within the triangle that encloses the point (t, p). For example, in Figure PORSURF- 2, the points constituting the lower triangle would be used for interpolation. As illustrated in Figure PORSURF- 3, this lower triangle can be divided into three sub-triangles that share the point (t, p). These sub-triangles have areas A_1, A_2, and A_3, while the larger triangle has area $A = A_1 + A_2 + A_3$. The porosity is then interpolated within the larger triangle as

$$\phi = \frac{A_1}{A}\phi(t_1, f_2) + \frac{A_2}{A}\phi(t_1, f_1) + \frac{A_3}{A}\phi(t_2, f_1)\ . \qquad \text{Equation (PORSURF.4)}$$

When $0 = t_1 \le t \le t_2$ (i.e., immediately after the operational period; see Appendix PA-2026, Section PA-4.2.3), the pressure $p(t_1, f)$ is zero for all f and the porosity $\phi(t_1, f)$ is equal to its initial value for all f, such that the lower triangle in Figure PORSURF- 2 would collapse to a line. The point (t, p) would, therefore, either fall within the upper triangle or above the interpolation data. In either case, the same methods described above would be used to interpolate and/or limit the value of $\phi(t, p)$.

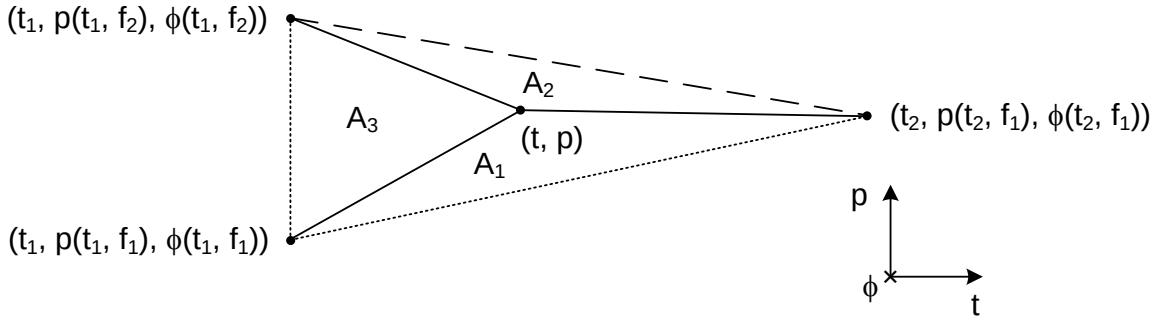


Figure PORSURF- 3. Triangular Interpolation to Determine the Porosity at (*t*, *p*)

Two further details should be noted. First, the interpolation uses 13 curves, rather than the 18 curves computed in Vignes et al. (2023). The 13 curves correspond to $f = 0$, 0.025, 0.05, 0.07, 0.085, 0.1, 0.15, 0.2, 0.3, 0.4, 0.6, 0.8, 1.0. Second, the Salado fluid flow simulations iteratively

solve for p at a given time, yet changes in p cause changes in ϕ, so ϕ is interpolated with each Salado fluid flow iteration to ensure that p and ϕ both converge together.

PORSURF-5.0 TREATMENT OF NON-WASTE-FILLED AREAS

In the face of the uncertainty surrounding the reconsolidation of non-waste-filled areas (see Appendix PORSURF-1.0), the PA uses the approach employed in all past compliance applications. During the development of the CCA PA, Vaughn et al. (1995a, 1995b) compared two models for non-waste filled areas: a fixed reconsolidation model, in which porosity was held low and permeability was held high, and a dynamic reconsolidation model, in which porosity and permeability varied with time and fluid pressure. They found that their fixed reconsolidation model predicted similar or higher radionuclide releases than their dynamic reconsolidation model. Soon after, the CCA PA assigned a fixed porosity of $\phi = 0.18$ and a fixed permeability of $k = 10^{-11}\ \mathrm{m}^2$ to the non-waste-filled areas (Butcher 1997, Section 3.5.1.2; Vaughn 1996). All subsequent compliance applications have used these values, including CRA-2026 (Kim and Feng 2023). This approach treats non-waste-filled areas as propped open by partially reconsolidated salt rubble and fluids.

Porosity and permeability typically trend together, so it is helpful to know that $\phi = 0.18$ and $k = 10^{-11}\ \mathrm{m}^2$ are reasonably consistent. Babcock and Stormont (2022, Figure 16) placed various samples of WIPP run-of-mine (ROM) salt in a permeameter, vibrated some samples to reduce their porosity, and measured their permeability. Extrapolating the measurements in the range of $0.27 \leq \phi \leq 0.43$ down to $\phi = 0.18$ results in $k \approx 10^{-10}\ \mathrm{m}^2$, which is close to $k = 10^{-11}\ \mathrm{m}^2$. Although this comparison is encouraging, one must regard it cautiously. Salt rubble and ROM salt likely have different hydraulic behaviors due to their different grain size distributions. In addition, mechanically deforming granular salt likely affects its hydraulic behavior differently than vibrating it.

A pair of recent sensitivity studies demonstrated the conservatism of treating non-waste-filled areas as open. The first study compared the CRA-2019 PA base case against a sensitivity calculation, named CRA19_CL (Zeitler et al. 2019, Appendix A). The CRA-2019 PA base case used $\phi = 0.18$ and $k = 10^{-11}\ \mathrm{m}^2$ for the non-waste-filled areas, whereas CRA19_CL adopted intact salt fluid flow properties ($0.001 \leq \phi \leq 0.0519$ and $10^{-24}\ \mathrm{m}^2 \leq k \leq 10^{-21}\ \mathrm{m}^2$, Kim and Feng 2019, Table 4) for the non-waste-filled areas. The CRA19_CL simulation showed a decrease in the mean total releases predicted in the CRA-2019 PA base case by factors of 0.83 and 0.53 at the 0.1 and 0.001 compliance limit probabilities, respectively. The second study was performed after the U.S Environmental Protection Agency (EPA) noted that the CRA19_CL analysis used typical fluid flow properties for the disturbed rock zone (DRZ) ($\phi = 0.0129$ and $k = 10^{-19}$ to $10^{-12.5}\ \mathrm{m}^2$) around the non-waste-filled areas. Consequently, the EPA replaced the non-waste-filled DRZ fluid flow properties with intact salt fluid flow properties and repeated the CRA19_CL calculation. This new calculation, named CRA19_COMP, further reduced the mean total releases predicted in CRA19_CL by factors of 0.96 and 0.89 at the 0.10 and 0.001 compliance limit probabilities, respectively (EPA 2022).

PORSURF-6.0 REFERENCES

(*Indicates a reference that has not been previously submitted.)

Babcock, E., and J. Stormont. 2022. Permeability and Porosity of Loose Granular Salt. Technical Report. University of New Mexico. EIMS-0005020799. *

Butcher, B. 1997. *Waste Isolation Pilot Plant Disposal Room Model.* Albuquerque, NM: Sandia National Laboratories. SAND97-0794.

Coussy, O. 2010. *Mechanics and Physics of Porous Solids*. Wiley. DOI: 10.1002/9780470710388. *

Day, B. 2025. *WIPP Repository Performance Impact as Attributed to Use of the New vs Legacy Porosity Surface for RPPCR*. Sandia Memorandum. EIMS-0004808327. *

Day, B., and S. King. 2025. *Analysis Report for Salado Flow in the 2026 Compliance Recertification Application Performance Assessment: Interim State Repository*. Revision 0. EIMS-0004944216. *

Freeze, G.A. 1996. *Repository Closure–Reasoned Argument for FEP Issue DR12*. Albuquerque, NM: Sandia National Laboratories. ERMS 413328.

Freeze, G.A., K.W. Larson, and P.B. Davies. 1995. *A Summary of Methods for Approximating Salt Creep and Disposal Room Closure in Numerical Models of Multiphase Flow*. Albuquerque, NM: Sandia National Laboratories. SAND94-0251.

Hansen, C., L. Brush, M. Gross, F. Hansen, B. Park, J. Stein, and T. Thompson. 2004. *Effects of Supercompacted Waste and Heterogeneous Waste Emplacement on Repository Performance, Revision 2*. WIPP Records Center, Carlsbad, NM: Sandia National Laboratories. ERMS 533551.

Jensen, R., S. Broome, C. Herrick, and B. Reedlunn. 2023. *Improved Compaction Experiments and Modeling of Waste Isolation Pilot Plant Standard, Non-degraded, Waste Containers*. Sandia National Laboratories. SAND2023-04823. *

Kim, S., and L. Feng. 2019. *Input Parameter Report for the 2019 Compliance Recertification Application Performance Assessment (CRA-2019 PA) Revision 1*. Carlsbad, NM: Sandia National Laboratories. ERMS 571660.

Kim, S., and L. Feng. 2023. *Input Parameter Report for the Replacement Panels Planned Change Request Performance Assessment (RPPCR PA) Revision 0*. Carlsbad, NM: Sandia National Laboratories. ERMS 579730. *

McCormick, J., R. Kirkes, and C. Hansen, 2024. *Conceptual Models in WIPP Performance Assessment*. Sandia National Laboratories. EIMS-0004385596. *

National Academy of Sciences-National Research Council (NAS-NRC). 1957. *The Disposal of Radioactive Waste on Land.* Publication 519. Washington, DC: National Academy of Sciences.

Park, B.Y., and F.D. Hansen. 2005. *Determination of the Porosity Surfaces of the Disposal Room Containing Various Waste Inventories for WIPP PA*. Sandia National Laboratories. SAND2005-4236. *

Park, B.-Y., and J. Holland. 2007. *Structural Evaluation of WIPP Disposal Room Raised to Clay Seam G*. Sandia NationalLaboratories. SAND2007-3334. *

Reedlunn, B., and J. Bean. 2019. *Simulations of Pipe Overpack Container Compaction at the Waste Isolation Pilot Plant*. Sandia National Laboratories. SAND2019-12111. *

Reedlunn, B., G. Moutsanidis, J. Baek, T.-H. Huang, J. Koester, E. Matteo, X. He, K. Taneja, H. Wei, Y. Bazilevs, J.-S. Chen, C. Mitchell, R. Lander, and T. Dewers. 2019. *Initial Simulations of Empty Room Collapse and Reconsolidation at the Waste Isolation Pilot Plant*. Sandia National Laboratories. SAND2019-15351. *

Reedlunn, B., J. G. Argüello, and F.D. Hansen. 2022. *A Reinvestigation into Munson's Model for Room Closure in Bedded Rock Salt*. International Journal of Rock Mechanics and Mining Sciences, 151, doi: 10.1016/j.ijrmms.2021.105007. *

Reedlunn, B., and J. Bean. 2024. *More Simulations of Criticality Control Overpack Container Compaction at the Waste Isolation Pilot Plant*. Memorandum. Sandia National Laboratories. SAND2024-07834CTF. *

Reedlunn, B., S. King, B. Day, C. Hamel, and J. Bean, 2025. *An Assessment of the Error Due to Computing Waste Isolation Pilot Plant Porosity Using the Porosity Response Surface Approach*. Albuquerque, NM: Sandia National Laboratories. SAND2025-12225.

Sierra/SolidMechanics. 2022. *Sierra/SolidMechanics 5.4 User's Guide*. Sandia National Laboratories, 5.4.1 edition, SAND2022-0103. *

Stone, C.M. 1997. *Final Disposal Room Structural Response Calculations*. Albuquerque, NM: Sandia National Laboratories. SAND97-0795.

U.S. Department of Energy (DOE). 1996. Title 40 CFR Part 191 Compliance Certification Application for the Waste Isolation Pilot Plant (October). 21 vols. Carlsbad, NM: Carlsbad Area Office. DOE/CAO 1996-2184.

U.S. DOE. 2019. Title 40 CFR Part 191 Subparts B and C Compliance Recertification Application for the Waste Isolation Pilot Plant, Carlsbad, NM: Carlsbad Field Office. DOE/WIPP 19-3609.

U.S. Environmental Protection Agency (EPA). 2022. Technical Support Document for Section 194.23, Review of the APCS Approach to Analyzing WIPP Repository Performance in the CRA-

2019 Performance Assessment. April 2022. Office of Radiation and Indoor Air. Docket: EPA-HQ-OAR-2019-0534-0050. *

Vaughn, P., M. Lord, and R. J. Mackinnon. 1995a. DR-3: Dynamic Closure of the North-End and Hallways; Summary Memorandum of Record to D.R. Anderson; Subject: FEP Screening Issue DR-3. Dated: December 21, 1995. ERMS 230794. Sandia National Laboratories.

Vaughn, P., M. Lord, and R. J. Mackinnon. 1995b. DR-7: Permeability Varying with Porosity in Closure Regions; Summary Memorandum of Record to D.R. Anderson; Subject: FEP Screening Issue DR-7. Dated: December 21, 1995. ERMS 230796. Sandia National Laboratories. *

Vaughn, P. 1996. Email to: melord, damcart, rjmacki, jebena, djschre, pvaughn; Northend Regions ('Backfill' and Experimental) Porosity; January 30th, 3:48 pm. ERMS 236320. Sandia National Laboratories. *

Vignes, C., J. Bean, and B. Reedlunn. 2023. *Improved Modeling of Waste Isolation Pilot Plant Disposal Room Porosity*. Sandia National Laboratories. SAND2023-04826. *

Zeitler, T.R., J. Bethune, S. Brunell, B. Day, D. Kicker, J. Long, and R. Sarathi. 2019. *Summary Report for the 2019 Compliance Recertification Application Performance Assessment (CRA–2019 PA)*. Carlsbad, NM: Sandia National Laboratories. ERMS 571376.